Electrodialytic remediation of municipal solid waste incineration fly ash as pre-treatment before geopolymerisation with coal fly ash

Zhan, Xinyuan; Kirkelund, Gunvor Marie

Published in:
Journal of Hazardous Materials

Link to article, DOI:
10.1016/j.jhazmat.2021.125220

Publication date:
2021

Document Version
Peer reviewed version

Title page:

Electrodialytic remediation of municipal solid waste incineration fly ash as pre-treatment before geopolymerisation with coal fly ash

Xinyuan Zhan[a,b], Gunvor Marie Kirkelund[a]

[a] Department of Civil Engineering, Technical University of Denmark, 2800 Lyngby, Denmark

[b] College of Environment and Ecology, Chongqing University, Chongqing, 400044, PR China

Corresponding author: Xinyuan Zhan, E-mail: 1520762208@qq.com

Department of Civil Engineering, Technical University of Denmark, 2800 Lyngby, Denmark

Contributions: Xinyuan Zhan: Conceptualization, Methodology, Validation, Writing- Original draft preparation, Writing-Reviewing and Editing. Gunvor Marie Kirkelund: Conceptualization, Supervision, Writing-Reviewing and Editing.

Acknowledgment: Xinyuan Zhan gratefully thanks the China Scholarship Council for the grant (CSC201906050008). Laboratory technicians Ebba Cederberg Schnell, Natasja Dueholm and PhD student Benjamin Alexander Regaard Ebert, Department of Civil Engineering, Technical University of Denmark are thanked for experimental and analytical help. Aase og Einar Danielsens Fond is acknowledged for funding the experimental work.

Electrodialytic remediation of municipal solid waste incineration fly ash as pre-treatment before geopolymerisation with coal fly ash

Xinyuan Zhan[a,b,*], Gunvor Marie Kirkelund[a]

[a] Department of Civil Engineering, Technical University of Denmark, 2800 Lyngby, Denmark

[b] College of Environment and Ecology, Chongqing University, Chongqing, 400044, PR China

* Corresponding author: zhanxinyuane@qq.com

Abstract

Municipal solid waste incineration (MSWI) fly ash is classified as hazardous waste and needs to be disposed of according to strict regulations. By disposal, valuable resources in the MSWI fly ash is lost, and other solutions are sought for. The effect of electrodialytic remediation (ED) as a pre-treatment for removing heavy metals from MSWI fly ash before using the treated ash in geopolymerization with coal fly ash was explored. ED pre-treatment for MSWI fly ash increased the Si reactivity and the Si/Al ratio. The mixture of 80% coal fly ash and 20% ED treated fly ash with 8M NaOH (L/S 0.37 mL/g) was found optimal, with a resulting compressive strength of 15.3 MPa, which was higher than the reference coal fly ash geopolymer. The leaching concentrations of Pb, Zn, Cr, Cu and Ni were below 0.02 mg/L with Mn and Cd at 0.023 and 0.027 mg/L, respectively. The enhanced mechanism for ED treated MSWI fly ash in geopolymer was confirmed by FTIR analysis and SEM images. The resistance against extreme leaching environments for treated fly ash geopolymer was stronger than raw fly ash geopolymer, and physical encapsulation of geopolymeric gels contributed to the heavy metal immobilization.

Keywords: MSWI fly ash; electrodialytic remediation; heavy metals; geopolymers; immobilization.

1. Introduction

Municipal solid waste incineration (MSWI) has become the mainstream method in waste management of household waste due to three advantages, namely energy recovery from waste, mass and volume reduction, and removal of pathogens. Accordingly, the by-product, MSWI fly ash (FA), is produced in large amounts. About 64 and 106.8 million tons of MSW are incinerated in EU by 2020 (CEWEP, 2013) and China by 2018 (China Statistical Yearbook, 2019). About 3% (Hjelmar et al., 2011) of the mass of incinerated MSW ends up as fly ash, corresponding to 1.92 and 3.06 million tons fly ash in EU and China. Meanwhile, the MSWI fly ash is classified as hazardous waste due to its considerable content in heavy metals, soluble salts and polychlorinated dibenzo-p-dioxins/furans (PCDD/Fs). Therefore, the FA must be disposed of before or further processed before alternative use. The European Commission encourages the circular economy, and MSWI fly ash as a secondary material plays a crucial role in promoting circular economy (Quina et al., 2018), but it needs to be pretreated. There are three main approaches for treatment before disposal or potential reuse of FA: recycling valuable elements by extraction (Quina et al., 2008, Luo et al., 2019), stabilization/solidification (S/S) (Zhan et al., 2019) and thermal treatment (Hwang et al., 2012).

The S/S method includes chemical agents immobilization, cement stabilization and other cementitious materials encapsulation (Shiddique, 2010; Wang et al., 2015; Mu et al., 2018; Atanes et al., 2019). Geopolymer, as a novel cementitious material, has received more attention in recent years for immobilizing heavy metals than other S/S approaches. FA can be utilized with red mud

(Ye et al., 2016), metakaolin (Jin et al., 2016), coal fly ash, mineral residues or other industrial solid waste containing aluminium and silicon resources which are necessary for geopolymerisation. The dominant S/S mechanism of heavy metals in FA is the gel mesh encapsulation in geopolymers (Li et al., 2019). The proportion of FA for preparing geopolymers was proposed at 5-15%, which cannot decrease the compressive strength and the durability of heavy metals in geopolymers (Lancellotti et al., 2010; Zhao et al., 2019). However, when the proportion of FA in geopolymers increased, the compressive strength of geopolymer containing FA decreased over time due to the high salts content (chlorides and sulfates)(Gunasekara et al., 2019), which could be problematic for the durability and mechanical performance of the geopolymers. Furthermore, FA has a low level of aluminium and silicon resources (Zheng et al., 2011) combined with a high content of soluble heavy metals, which indicates that it is not a proper material for geopolymerisation in its raw state. Therefore, FA must be pretreated to improve its properties when used in geopolymerization and following enhancing the performance of MSWI fly ash-based geopolymers. Furthermore, the recycling proportion of FA after pretreatment in geopolymers can be increased.

Electrodialytic remediation is an extraction and separation method that can remove toxic metals from contaminated materials (Kirkelund et al., 2019). The contaminated material is suspended in distilled water in a suspension compartment which is separated from the electrolyte compartments by ion-exchange membranes. The metals are extracted from the material due to acidification processes in the electrodialytic cell, and ionic metal species are separated from the suspenions compartment to the electrolytes by electromigration in an applied electric field. The total amounts of SiO_2 and Al_2O_3 for a Greenlandic FA increased from 8.1% to 17.1% by electrodialytic remediation (Kirkelund et al., 2018), and it reduced the chloride and soluble heavy

66 metals content (Belmonte et al., 2018). Thus, the result showed that electrodialytic remediation is
67 a potential pre-treatment method for FA.

68 In this work, electrodialytic remediation was used as a pre-treatment method to improve the
69 chemical properties of FA before the utilization in coal fly ash geopolymerisation. The
70 experimental outcome of the electrodialytic remediation was analyzed, especially for the heavy
71 metals and chlorides. The difference between the pretreated and raw FA used in geopolymerisation
72 was studies for mechanical and environmental properties. It was finding that the electrodialytic
73 remediation for FA increased by 33.3% in the recycling proportion in geopolymers.

74

75 2. Materials and methods

76 2.1 MSWI fly ash and coal fly ash collection

77 MSWI fly ash (FA) in this study was from Amager Bakke MSWI plant of Copenhagen,
78 Denmark. Coal fly ash (CFA) was collected from a coal power plant in Chongqing, China and
79 classified as ASTM Class F fly ash.

80 2.2 Electrodialytic remediation experiments

81 The electrodialytic remediation (ED) apparatus was built with three compartments, as shown
82 in Fig.1. The ED apparatus was made up of two 5 cm long cylinders with an inner diameter of 8
83 cm (electrolyte chambers I and III) and a 10 cm long cylinder in between (suspension chamber II).
84 The anion exchange membrane (AN) and cation exchange membrane (CAT) were placed between
85 the electrode (chamber I and III) and the middle chamber (II), respectively. Chambers I and III
86 were the anode and cathode compartments and filled with 500 mL circulating electrolytes of a 0.01
87 M $NaNO_3$ solution with a pH of 2 adjusted by HNO_3. The ash suspension with 100 g FA and 350

88 mL distilled water in chamber II was automatically stirred. Some details concerning the ED
89 experiment were as follows:

90 ● Power supply: A DC power supply (Hewlett Packard E3612A) kept a constant current of 50
91 mA and monitored the voltage variation between the cathode and anode.
92 ● Electrodes: The electrodes were obtained from Permascand and made of platinum-coated
93 titanium wires with a diameter of 3 mm.
94 ● Electrolyte circulation in chamber I and III: A peristaltic pump was applied to circulate
95 electrolyte of the electrode compartment. Water flux (Lima et al., 2008) occurred over ED
96 experiment and reduced by adjusting the pump rate.
97 ● Exchange membrane: The ion exchange membranes were obtained from Ionics (anion
98 exchange membrane 20 SZRA B02249C and cation exchange membrane CR67 HUY
99 N12116B).
100 ● Stirring: A flexible plastic flap fastened on a glass rod was put in chamber II. The glass stick
101 was fixed into an overhead stirrer.
102 ● Control and measurement during the ED experiment: The pH and electrical conductivity of
103 ash suspension and voltage drop between electrodes were determined and recorded daily. The
104 catholyte and anolyte were kept the pH at 1-2 by adjusting with 6M NaOH solution in the
105 anolyte and 8M HNO_3 solution in the catholyte. The whole ED experiment lasted 28 days and
106 was conducted at ambient temperature.
107 ● After ED experiment: the ash suspension was filtered through a 45 μm filter and the treated
108 material dried at 105ºC before further digestion and heavy metal analysis. The membranes
109 and stirrer were placed in 1 M HNO_3 and the electrodes in 5 M HNO_3. All liquid samples,

including suspension liquid and electrolytes were kept for heavy metal analysis and the ED treated fly ash (TFA) was used for geopolymer samples.

.

2.3 Geopolymer preparation

The geopolymer mixes are shown in Table 1. The raw materials were blended for 5 min to acquire homogeneity and then stirred manually with 8 M NaOH solution (L/S ratio of 0.37 mL/g) for 10 min. The mixture was poured into rubber moulds (20*20*20 mm) and entrapped air bubbles were removed through vibration (5 min). The moulds were kept in a curing box at 80 °C and cured for 24 hours. The samples were demoulded after 24 hours and cured for 7 and 28 days at ambient temperature and humidity. Leaching tests, compressive strength, XRD, FTIR and SEM analysis of S/S solids were conducted.

2.4 Analytical tests

Based on Technical specification for pollution control of fly-ash from municipal solid waste incineration (HJ 1134—2020), leaching method of HJ 557-2010 was used to assess the leaching behavior of heavy metals in raw materials and geopolymers samples (Table 1) and performed for three repetitions. Four grams of fly ash sample was mixed with 40 mL distilled water (L/S = 10 mL/g), and the samples were horizontally shaken at 110 $\pm$ 10 rpm/min and an amplitude of 40 mm for 8 h at ambient temperature; after that, the samples were kept stationary for 16 h and the pH of suspensions was measured, and then the solutions were filtered before Cd, Cu, Cr, Zn and Pb were analysed by ICP-OES (Varian 720-ES, USA). Cl anion was determinted on the leaching solution by ion chromatography (Dionex ICS-1100, Thermo Scientific, USA). Each leaching test was characterized by mean and deviation values. The acid-alkaline against experiments of FA, CFA20FA and CFA20TFA geopolymers were conducted in accordance with the method of HJ

557-2010 for two blinds, but the leaching solutions were 0.01, 0.05, 0.1, 0.3, 0.5, 1 M HNO_3, 0.5 and 1 M NaOH solutions, respectively. The reactivity of Al and Si in the raw materials was determined based on the methods reported by Panagiotopoulou et al. (2007) and conducted in three replicates. One g sample was dissolved in 40ml 10M NaOH solution and the mix was shaken for 24 hours at 20 and 80 °C, whereafter 2 ml leachate was diluted to 20 ml, filtrated and acidified with 2 ml concentrated HNO_3. The samples were stored at 4°C before Al and Si were analysed by ICP-OES.

Mineral phases of raw materials and the composite geopolymers were assessed by use of XRD (X'Pert Pro, PANalytical, Netherlands) with CuKa radiation in the 2θ range from 10° to 80° at a scanning rate of 0.02°/s for 2h. The data of XRD was analyzed by Jade 5.0 and the crystallinity of samples was calculated based on built-in silicon data of Highscore Plus. Raw materials and geopolymers were measured between 4000 and 600 cm-1 by use of FTIR (Spotlight 400, PerkinElmer, USA). The micro-morphology of raw materials and geopolymers were tested on powder samples by use of SEM (Quanta 250, FEI, USA). The major elements of the raw materials were determined by the use of XRF (XL3t, Thermo Scientific Niton Co., US). Chinese Standard GB/T 17671-1999 (GB/T 17671, 1999) were used as a guideline to test the compressive strength of samples and an Instron 6025 was used for this purpose on three replicates of the mixtures seen in Table 1.

3. Results and discussion

3.1 Electrodialytic experiment

The pH and electrical conductivity of the FA suspension, along with the voltage drop over the ED cell are presented in Fig. 2. The pH of the fly ash suspension decreased during the ED experiment due to the acidification by the water splitting at the anion exchange membrane. The electrical conductivity of the suspensions first decreased and then increased. The former was explained by that the hydroxyl anion is the most conductive and when it is neutralized by protons the conductivity decreases, and the latter increase was due to the constitutes of FA dissolving during the acidification of the suspension. The voltage drop of the ED system was almost kept constant at 4V, indicating that the energy this pre-treatment method needed was at a low level owing to the low consuming power (UI). The final distribution of heavy metals in the ED system is shown in Fig. 3 and the details in the Table S1. The removal rates of Cd, Cu, Mn and Zn (the amount of the metal except what remains in treated ash) were 98%, 80%, 78% and 84%, respectively, higher than that of Cr (36%), Ni (45%) and Pb (12%). For Cd, Cu, Mn and Zn, the major amounts were in the cathode side of the electrodialytic cell, which means that these metals were mainly removed as cations (Cd^{2+}, Cu^{2+}, Mn^{2+} and Zn^{2+}). In contrast, the Pb and Cr mainly remained in the TFA, which indicates that the major type of Pb and Cr in FA belongs to acid-insoluble fractions. For Pb, Pb^{2+} ions dissolving from FA can react with the SO_4^{2-} to the insoluble $PbSO_4$. The proportion of Pb found in the anolyte was higher than other heavy metals, which means that Pb also formed anions, such as PbO_3^{2-}, $Pb_2Cl_5^-$ and $PbCl_4^{2-}$ (Jiao et al., 2016). The pH of the ash suspension at the end of the electrodialytic experiment was 1.63. The metal proportion found in the ash suspension at the end of the experiment that had not electromigrated to the electrode chamber indicates that the heavy metals in the filtrate from ash suspension were in the

175 form of neutral metal complexes or may be in non-soluble solid phases. For instance, 18 % Cr was
176 found in ash suspension, suggesting uncharged Cr metal complexes such as non-soluble chromate
177 or dichromate compounds (Ščancar and Milacic, 2014).

178 3.2 Characteristics of CFA, FA and TFA.

179 The chemical composition and leaching characteristics of CFA, FA and TFA are shown in
180 Table 2. The CFA contained large amounts of aluminium-silicate resources, which indicate that
181 the CFA is an eligible geopolymer material. In contrast, the FA was mainly composed of chlorides,
182 sulfates and Ca-bearing compounds, in which chlorides prevent FA from being a high-grade
183 material for geopolymerization. After ED pretreatment for FA, silicon in TFA increased and
184 chloride decreased, which was beneficial to the geopolymeric reaction due to more formation of
185 $Si[OH]_4^-$ (Li et al., 2019). The FA had large quantities of heavy metals like Zn, Pb, Cd, Cu, Cr,
186 Mn and Ni compared with coal fly ash, as well as for Cl^- ions. Based on the leaching test, it was
187 found that the leaching concentrations of heavy metals in FA were low except the Pb and Zn. This
188 can be explained by that the alkaline property of FA caused the heavy metals to form hydroxide
189 compounds and precipitate on the FA particles. However, the Pb leaching concentration exceeded
190 1 mg/L, limit value of GB 8978-1996. The heavy metal concentrations for TFA were lower than
191 for raw MSWI FA except for Pb. The most significant decrease in concentrations was seen for Cd,
192 Cu, Mn and Zn. Based on Fig. 3, the soluble metals in the fly ash were dissolved into the
193 suspension and the majority of the metal ions migrated to the cathode. Thus, the increase of Pb
194 concentration for TFA is explained by that 44 % of the ash dissolved in the ED experiment and
195 this dissolution was mainly due to the soluble salts. The leaching concentrations of heavy metal in
196 treated fly ash were higher than that of the raw fly ash, and exceeded the limit value of GB 8978-
197 1996 for Cd, Cu, Ni, Pb and Zn. The main factor causing the leaching increase was the final pH of

198 the leaching solution which was for treated fly ash which was acidic (pH 4.7) compared to the
199 alkaline (pH 11.9) for the untreated fly ash. However, the leaching concentration of Cr and Pb
200 decreased for the TFA due to the formation of their non-soluble compounds.

201 The Al and Si reactivity of the raw materials used for geopolymerisation is shown in Table 3
202 and all materials contained reactive Al and Si. The reactive Al and Si of the FA and TFA was
203 similar or even higher than of the CFA at ambient temperatures. The reactive Al and Si
204 concentration increased with higher temperature, which has also been found for metakaolin
205 (Granizo et al., 2014) and gold mine tailing (Falayi, 2019). Note that the increase in Si reactivity
206 for CFA at 25 and 80 °C was two times the reactivity of Al, which means that the reactive Si/Al
207 ratio under high temperature increases and this could favor the development of compressive
208 strength for CFA geopolymers (Tzanakos et al., 2014). TFA contained more reactive Si and less
209 reactive Al compared to FA, so that the ratio of reactive Si/Al increased after electrodialytic
210 treatment of the fly ash.

211 The crystalline phases of CFA, FA and TFA were determined by XRD and are shown in Fig.
212 4. CFA contained the crystal minerals of mullite (PDF#15-0776), quartz (PDF#46-1045), calcite
213 (PDF#05-0586) and hematite (PDF#33-0664) with low total crystallinity of 5%. The low
214 crystallinity combined with the chemical composition of coal fly ash, indicated that most
215 aluminium silicate resources of CFA were amorphous. In contrast, the crystalline phases of the FA
216 were mainly anhydrite (PDF#37-1496), halite (PDF#05-628), quartz, calcite and hematite
217 (PDF#33-0664) and of the TFA were mainly anhydrite, bassanite (PDF#41-0224) and quartz. A
218 significant difference between FA and TFA, was that NaCl was removed due to the electrodialytic
219 treatment and this is confirmed by the reduced chloride leaching in Table 2. It can be expected that

220 alkaline Ca-bearing compounds in FA such as anhydrite, bassanite and calcite can promote the
221 geopolymeric reaction of CFA geopolymers (Zhan et al., 2018).

222 3.3 CFA based geopolymer with FA and TFA

223 The compressive strength of geopolymers with FA and TFA is shown in Fig. 5. When the
224 proportion of FA in the geopolymer was 5 - 15% and cured for 7 days, there was no obvious effect
225 on the compressive strength. However, the increase of FA deteriorated the compressive strength
226 of geopolymers at 28 days of curing. This result indicates that the FA can be a potential substitute
227 for CFA at low proportion and consistent with the result reported by Tian et al. (2020). Meanwhile,
228 with 20% FA in the geopolymer, the compressive strength of CFA-FA geopolymer decreased and
229 further decreased when using 25% FA. When using the TFA, a proportion of 15 and 20% TFA in
230 the geopolymer resulted in similar or higher compressive strengths as the CFA and CFA-FA
231 geopolymers with up to 15% FA. This difference between the FA and TFA geopolymers can be
232 explained by that the FA contains considerable amounts of soluble salts and less aluminum-silicate
233 resources while the the Si reactivity for the TFA increased and the reactive Al decreased (Table
234 3). Furtheremore, the reactive Al concentration of TFA decreased and it was observed that fewer
235 bubbles emerged during the preparation of geopolymers with TFA than with FA, which could be
236 due to that metallic aluminum of FA decreased after ED pre-treatment. Metallic aluminum in
237 FA is not normally measured, due to difficulties in measurements. However, Aubert et al. (2004)
238 reported the FA has about 0.2% metallic aluminum, and metallic aluminum is detrimental in
239 geopolymer preparation and metallic aluminum can result in more pores in the geopolymers due
240 to H_2 released (Tian et al., 2020). Therefore, the soluble salts, low content in aluminum-silicate
241 and metallic Al contributed to the difference of CFA-FA and CFA-TFA geopolymers. The

242 CFA20TFA was the optimal for preparing geopolymers, reaching 15.3 MPa for curing 28 days
243 and similar as CFA geopolymer.

244 3.4 Characterization of geopolymers

245 The XRD diffractograms of the geopolymers are shown in Fig. 6. The low crystallinity (5-
246 6 %) in all geopolymer samples indicate that the geopolymer reaction has occurred. In GP-CFA,
247 the peak of mullite decreased and the peak of zeolite ($Na_8(AlSiO_4)_6CO_3$) appeared, along with the
248 decrease of geopolymer crystallinity compared to the diffractogram of the CFA itself (Fig. 5). The
249 zeolite was considered as resulting from the geopolymer process and can co-exist with geopolymer
250 products (Rozek et al., 2019). However, the mineral phases of CFA20FA geopolymer were
251 complex and composed of zeolite, mullite, thenardite, quartz, calcium silicate hydrate, thaumasite,
252 hematite, halite and dellaite, which can be explained by the NaOH reacting with FA, that consists
253 of considerable impurities. In contrast, the diffraction peak of thenardite (Na_2SO_4) for CFA20TFA
254 geopolymer increased without other sulfate-bearing phases, and TFA contained considerable
255 amounts of gypsum ($CaSO_4$), thus this phenomenon indicates more calcium (Ca) involved in the
256 geopolymerization. The original zeolite ($Na_8(AlSiO_4)_6CO_3$) derived from CFA geopolymer
257 disappeared in CFA20TFA and a new zeolite ($Na_8(Al_6Si_6O_{24})S_2O_3 \cdot 3H_2O$) was formed, which
258 means that TFA can inhibit the form of original zeolite and more amorphous geopolymeric gels
259 are formed.

260 Fig. 7 shows the FTIR spectra of raw materials (CFA, FA and TFA) and geopolymers (GP-
261 CFA, CFA20FA and CFA20TFA). In Fig. 6, one broad peak at 1096 cm^{-1} of CFA FTIR spectrum
262 was ascribed to stretching vibrations of T-O (T = Al or Si) bonds (Fernández-Jiménez and Palomo,
263 2005). The bands at 1412 cm^{-1} and 875 cm^{-1} of FA were attributed to symmetric stretching
264 vibrations of O-C-O bond indicating the existence of carbonates (CO_3^{2-}) (Jin et al., 2016). The

band frequencies at 1730 cm^{-1} and 3606 cm^{-1} in TFA were assigned to asymmetric O-H stretching vibration. An intense and broad band of S-O at 1110 cm^{-1} with a minor band at 659 cm^{-1} due to SO_4^{2-} (Lanzon and Garcia-Ruiz, 2012) were also observed in the TFA infrared spectra, which shows the existence of gypsum, consistent with the results of XRD. The bond frequencies of T-O in geopolymers exhibited a bathochromic shift (lower wavenumbers) of about 136 cm^{-1} from 1096 to 960 cm^{-1} compared to the raw materials, revealing that the vitreous component of raw materials was reacting with the alkali activator and formed the alkaline aluminosilicate gel (Fernández-Jiménez and Palomo, 2005). Furthermore, the characteristic asymmetric stretching vibration of Al-O and Si-O for reported geopolymers (Jin et al., 2016; Gunasekara et al., 2019) occurred at the peaks in the range of 900 cm^{-1} and 1000 cm^{-1}, which is also consistent with what was seen in this study. However, the stretching band (962 cm^{-1}) of Si-O-T (T = Al or Si) was affected by the addition of MSWI fly ash in the geopolymer. With the addition of FA and TFA, it shifted from 962 cm^{-1} to 960 cm^{-1} (CFA20FA) and 967 cm^{-1} (CFA20TFA). The blue-shift (higher wavenumbers) of the stretching bond of Si-O-Al (Si) in CFA20TFA compared with GP-CFA indicates that the heavy metals influenced the molecular structure of geopolymers and incorporated in the gels (Huang et al., 2018).

To further explore the geopolymeric mechanism of geopolymers and the difference on the raw and treated fly ash geopolymers, SEM pictures of the raw materials and geopolymers (cured for 28 d) are presented in Fig. 8. The microstructure of FA consisted of massive flocculus, while the TFA demonstrated large amounts of crystal minerals and this is inagreement with the high crystallinity result of the XRD. The micro-morphology of CFA was made up of smooth round particles and some impurities (like unburn carbon). By contrast, there were some rough round particle in GP-CFA geopolymer, which was reacted by the NaOH to form geopolymer gels (Jin et

al., 2016). Note that the reacted round particle of CFA20FA had severe reaction with smooth surface and its geopolymer gel was layered with micro particles around the geopolymer gel. Compared with CFA20FA geopolymer, the geopolymer gel of CFA20TFA tightly stuck on the reacted rough round particles (Jiang et al., 2020), and the microstructure was denser than CFA20FA, which further indicate why the compressive strength of CFA20TFA geopolymer was higher.

3.5 pH-desorption of heavy metals in FA and geopolymers

The leaching from the geopolymers is shown in Table 4. The metal leaching from all samples was generally low and not detected (< 20μg/l) and no clear trends were seen in metal leaching with increased fly ash proportion in the geopolymers. The pH in leaching solutions for geopolymers was highly alkaline and higher than the pH in the leaching solution of the FA and TFA. The leaching pH decreased in the 28 days cured samples compared to 7 days, which indicates that the geopolymerisation process continued and the aluminum-silicate, consumed OH^- ions to form geopolymeric gels in the form of $Si[OH]_4^-/Al[OH]_4^-$. The final pH of leaching solution for CFA-TFA geopolymers was slightly lower for all samples except for the sample CFA25TFA cured for 28 days, where pH was 12.4. This indicates that the lower pH of the TFA also influenced the pH of the geopolymers. The Cd, Ni, Zn, Cu, Mn and Cr leaching concentrations for CFA-25FA geopolymers increased over time, which indicate that the highest FA addition reduced the stabilizing capacity of heavy metals in the geopolymers. Contrarily, the Cd, Ni and Mn leaching behaviours of CFA-TFA geopolymers showed reduced leaching from 7 to 28 days, indicating that the ED pre-treatment for FA can enhance the stabilizing capacity of heavy metals for the geopolymers. The Cl leaching concentration of CFA-TFA geopolymers was lower than that of

311 CFA-FA geopolymers. Based on the leaching results, the proportion of 20% TFA for geopolymers
312 seems optimal. The leaching concentration of Pb, Zn, Cu and Mn for CFA20TFA was lower than
313 that of CFA20FA, and all heavy metals leaching concentration met the heavy metals control
314 standard of GB 8978-1996. The leaching concentrations of Pb, Zn, Cr, Cu, Ni and Mn in
315 CFA20TFA were below the detection limit with Mn and Cd below the control limit (GB8978-
316 1996). The leaching of heavy metals for geopolymers would mainly result from the FA and TFA,
317 rather than the CFA. Therefore, the mobility index (Kirkelund et al., 2020) of the geopolymers
318 was calculated in Table 5. If mobility index is below 1, indicating an immobilization of heavy
319 metals in geopolymers, and above 1 a mobilization. The mobility index of Cr, Zn and Pb for CFA-
320 FA geopolymers were below 1 at curing 28 days. In comparison with that, the mobility index of
321 Mn, Cd, Zn, Pb, Ni and Cu for CFA-TFA geopolymers were below 1. Therefore, more heavy
322 metals can be incorporated in CFA-TFA geopolymers. Note that the mobility index of Cr, Cd, Mn,
323 Zn, Pb, Ni and Cu for CFA20TFA geopolymer was the lowest among geopolymers and reduced
324 along with curing times, indicating that its stabilizing capacity of heavy metals was strong and
325 stable.

326 Fig. 9 shows the leaching behavior of heavy metals for FA, CFA20FA and CFA20TFA
327 geopolymers under alkaline and acidic conditions. From Fig. 8a, it can be seen that the Pb, Zn and
328 Cu showed a similar V-shaped desorption trend. The leaching behaviors of Pb and Zn for various
329 pHs were due to their amphoteric properties, while that of Cu was due to the form of CuO_2^{2-}
330 /$[Cu(OH_4)]^{2-}$ at alkaline pH. Cd, Mn and Ni mainly leached at acidic pH. In contrast, the Cr
331 leaching behavior had the least fluctuation range, especially between the pH of 0.5 and 14. The
332 metal leaching behavior from the geopolymers was different than the FA. The leaching
333 concentration of heavy metals for CFA20FA geopolymer (Fig. 9 b) showed a plateau with limited

leaching between pH 1 and 7 and demonstrated a U-shape trend, especially for Zn, Pb and Cu. This indicates a strong stabilizing capacity of heavy metals in the acidic environment for the geopolymer, than for the FA, which started leaching of metals at pH 2. This is probably due to a higher acid-base buffering capacity in the geopolymers. The leaching behaviors of heavy metals in CFA20FA geopolymer was similar to that of FA, but the leaching concentrations of heavy metals in CFA20FA geopolymer were lower than that of FA, as expected, since the total amount of heavy metals was lower in the geopolymers. For CFA20TFA geopolymer (Fig. 9c), the leaching concentration of heavy metals is lower than for CFA20FA (Fig. 9b) and especially at the strong acidic environment, which suggests that the durability in an extreme acidic environment for CFA20TFA is stronger than for CFA20FA, and this can be explained by the heavy metals could be incorporated in the geopolymeric gels as the blue-shift of the stretching bond of Si-O-Al(Si) (Fig. 7).

3.6 Economic analysis

In this work, FA was pretreated by ED system and put in CFA geopolymer. In order to further apply this method, the cost analysis of this method was assessed. The costs of human resource, labor, materials transportion and equipment depreciation were not taken into consideration, only for energy consumption and chemical reagents cost. The energy consumption can be calculated as (Oliveira et al., 2019):

$$E = \int V \times I dt$$

where E is the energy consumption (Wh), V is the voltage variation between electrodes (V), I is the current (A) and t is duration (h). Therefore, the energy consumption of ED system was 1.41 KWh for 1 kg MSWI fly ash. Based on the average price in Chinese market, the commercial price of NaOH is $ 257.1/t and the electricity cost is $ 0.07/KWh. According to above results, 200 kg

TFA and 800 kg CFA needs 160 kg NaOH, thus the cost of producing geopolymers needs $ 52.5/t. But, the more energy consumption was due to the stirrer in ash suspension (Oliveira et al., 2019). Due to the first time to use this method and lacking of pilot experiment, the energy consumption of stirrer need to further consider. Therefore, the reduction of energy consumption for stirrer and duration should be further researched, like reducing duration time and using pulse stirrer next.

4. Conclusion

The removal rates of Cd, Cu, Mn and Zn for TFA were higher than that of Cr, Ni and Pb. ED remediation alone for FA increased the leaching concentrations of Cd, Cu, Mn, Ni and Zn, even though the total heavy metal concentration was reduced. The leaching concentrations of heavy metals from the FA were low, except the Pb and Zn.The ED pre-treatment for FA improves the Si reactivity, not just the Si total content, along with an increase in the Si/Al ratio. The compressive strength of CFA20TFA was higher than that of CFA20FA geopolymer and reached 15.3 MPa for curing 28 days, which revealed that the ED pre-treatment for FA could upgrade its quality as precursor for geopolymer and increase its recycling potential. The leaching concentrations of Pb, Zn, Cr, Cu, Ni and Mn in CFA20TFA were below the detection limit with Mn and Cd below the control limit. The original zeolite ($Na_8(AlSiO_4)_6CO_3$) derived from CFA geopolymer disappeared in CFA20TFA, meaning that TFA can inhibit the formation of original zeolite and form more amorphous geopolymeric gels. The blue-shift (higher wavenumbers) of the stretching bond of Si-O-Al (Si) in CFA20TFA compared with GP-CFA indicates that the heavy metals had influenced the molecular structure of geopolymers and incorporated in the gels. Compared with CFA20FA geopolymer, the geopolymer gel SEM of CFA20TFA tightly sticked on the round particles, and the microstructure was denser than CFA20FA. The durability against extreme environment of CFA20TFA was stronger than CFA20FA and physical encapsulation of geopolymeric gels

contributed to the heavy metal immobilization. The electrodialytic remediation for MSWI fly ash increased by 33.3% in the recycling amount in coal fly ash geopolymers.

Acknowledgements

Xinyuan Zhan gratefully thanks the China Scholarship Council for the grant (CSC201906050008). Laboratory technicians Ebba Cederberg Schnell, Natasja Dueholm and PhD student Benjamin Alexander Regaard Ebert, Department of Civil Engineering, Technical University of Denmark are thanked for experimental and analytical help. Aase og Einar Danielsens Fond is acknowledged for funding the experimental work.

Reference

Atanes, E., Cuesta, B., Nieto, A., Fernandez, F., 2019. A mixed separation-immobilization method for soluble salts removal and stabilization of heavy metals in municipal solid waste incineration fly ash, Journal of Environmental Management, 240:359-367.

Aubert, J.E., Husson, B., Vaquier, A., 2004. Metallic aluminum in MSWI fly ash: quantification and influence on the properties of cement-based products. Waste Management, 24: 589-596.

Belmonte, L.J., Ottosen, L.M., Kirkelund, G.M., Jensen, P.E., Andreas Peter Vestbø., 2018. Screening of heavy metal containing waste types for use as raw material in arctic clay-based bricks. Environmental Science and Pollution Research, 25(33):32831-32843

CEWEP (2013): A decade of Waste-to-Energy in Europe (2001-2010/2011), Confederation of European Wasteto-Energy Plants (CEWEP), Brussels, Belgium

China Statistical Yearbook. National Bureau of Statistics of China, available from: < http://www.stats.gov.cn/tjsj/ndsj/2019/indexch.htm>, 2019.

Chinese Ministry of Environmental Protection. Method HJ557-2010: Solid Waste-Extraction procedure for leaching toxicity-Horizontal vibration method. China Environment Science Press, Beijing, China, 2010.

Chinese Ministry of Environmental Protection. HJ 1134-2020: Technical specification for pollution control of fly-ash from municipal solid waste incineration. China Environment Science Press, Beijing, China, 2020.

CN-GB, Method of testing cements-Determination of strength (GB/T17671-1999), 1999.

CN-GB, Integrated wastewater discharge standard (GB8978-1996), 1996.

Falayi, T., 2019. Effect of potassium silicate and aluminate on the stabilisation of gold mine tailings. Proceedings of the Institution of Civil Engineers - Waste and Resource Management, 172(2):56-63

Fernández-Jiménez, A., Palomo, A., 2005. Composition and microstructure of alkali activated fly ash binder: effect of the activator, Cement and Concrete Research, 35 (10): 1984-1992.

Galiano, Y.L., Pereira, C.F., Vale, J., 2011. Stabilization/solidification of a municipal solid waste incineration residue using fly ash-based geopolymers. Journal of Hazardous Materials, 185: 373-381.

Gunasekara, C., Law, D., Bhuiyan, S., Setunge, S., Ward, L., 2019. Chloride induced corrosion in different fly ash based geopolymer concretes. Construction and building materials 200:502-513.

Granizo, N., Palomo, A., Fernandez-Jimenez, A., 2014. Effect of temperature and alkaline concentration on metakaolin leaching kinetics. Ceramics International 40:8975–8985.

Hjelmar, O., Johnson, A., Comans, R., 2011. Incineration: solid residues. In: Christensen TH (ed) Solid waste technology & management. Wiley, p 430–462.

Huang, X., Muhammad, F., Yu, L., Jiao, B.Q., Shiau, Y., Li, D.W., 2018. Reduction/immobilization of chromite ore processing residue using composite materials based geopolymer coupled with zero-valent iron, Ceramics International, 44: 3454-3463.

Hwang, C., Bui, L., Lin, K., Lo, C., 2012. Manufacture and performance of lightweight aggregate from municipal solid waste incinerator fly ash and reservoir sediment for self-consolidating lightweight concrete. Cement and Concrete Composites, 34(10):1159-1166.

Jiao, F., Zhang, L., Dong, Z., Namioka, T., Yamada, N., Ninomiya, Y., 2016. Study on the species of heavy metals in MSW incineration fly ash and their leaching behavior. Fuel Processing Technology 152:108–115.

Jiang, X., Zhang, Y., Xiao, R., Polaczyk, P., Zhang, M., Hu, W., Bai, Y., Huang, B., 2020. A comparative study on geopolymers synthesized by different classes of fly ash after exposure to elevated temperatures. Journal of Cleaner Production, 270: 122500.

Jin, M., Zheng, Z., Sun, Y., Chen, L., Jin, Z., 2016. Resistance of metakaolin-MSWI fly ash based geopolymer to acid and alkaline environments. Journal of Non-Crystalline Solids, 450:116–122.

Lancellotti, I., Kamseu, E., Michelazzi, M., Barbieri, L., Corradi, A., Leonelli, C., 2010. Chemical stability of geopolymers containing municipal solid waste incineration fly ash. Waste Management, 30: 673-679.

Lanzon, M., Garcia-Ruiz, P.A., 2012. Effect of citric acid on setting inhibition and mechanical properties of gypsum building plasters, Construction and Building Materials, 28:506-511.

Li, Y., Min, X., Ke, Y., Liu, D., Tang, C., 2019. Preparation of red mud-based geopolymer materials from MSWI fly ash and red mud by mechanical activation. Waste Management, 83: 202-208.

Lima, A.T., Ottosen, L.M., Ribeiro, A.B., Hansen, H.K., 2008. Electrodialytic removal of Cd from straw ash in a pilot plant. Journal of Environmental Science and Health Part A, 43: 844–851.

Luo, H., Cheng, Y., He, D., Yang, E.H., 2019. Review of leaching behavior of municipal solid waste incineration (MSWI) ash, Science of the Total Environment, 668:90-103.

Kirkelund, G.M., Jensen, P.E., 2018. Electrodialytic treatment of Greenlandic municipal solid waste incineration fly ash. Waste Management, 80: 241-251.

Kirkelund, G.M., Jensen, P.E., Ottosen, L.M., Pedersen, K.B., 2019. Comparison of two- and three-compartment cells for electrodialytic removal of heavy metals from contaminated material suspensions. Journal of Hazardous Materials, 367: 68-76.

Kirkelund, G.M., Skevi, L., Ottosen, L.M., 2020. Electrodialytically treated MSWI fly ash use in clay bricks. Construction and Building Materials, 254:119286

Mu, Y., Saffarzadeh, A., Shimaoka, T., 2018. Influence of ignition of waste fishbone on enhancing heavy metal stabilization in municipal solid waste incineration (MSWI) fly ash, Journal of Cleaner Production, 189:396-405.

Oliverira, V., Kirkelund, G.M., Horta, C., Labrincha, J., Dias-Ferreira, C., 2019. Improving the energy efficiency of an electrodialytic process to extract phosphorus from municipal solid waste digestate through different strategies, Applied Energy, 247: 182-189.

Panagiotopoulou, Ch., Kontori, E., Perraki, Th., Kakali, G., 2007. Dissolution of aluminosilicate minerals and by-products in alkaline media. Journal of Material Science, 42:2967-2973.

Rozek, P., Krol, M., Mozgawa, W., 2019. Geopolymer-zeolite composites: A review. Journal of Cleaner Production, 230:557-579.

Quina, M., Bontempi, E., Bogush, A., Schlumberger, S., Weibel, G., Braga, R., Funari, V., Hyks, J., Lederer, J., 2018. Technologies for the management of MSW incineration ashes from gas cleaning: New perspectives on recovery of secondary raw materials and circular economy. Science of The Total Environment, 635:526-542.

Quina, M., Bordado, J., Quinta-Ferreira, R., 2008. Treatment and use of air pollution control residues from MSW incineration: An overview. Waste Management, 28:2097-2121

Šcˇancˇar, J., Milacˇicˇ, R., 2014. A critical overview of Cr speciation analysis based on high performance liquid chromatography and spectrometric techniques. J. Anal. At. Spectrom. 29, 427.

Siddique, R., 2010. Utilization of municipal solid waste (MSW) ash in cement and mortar, Resources, Conservation and Recycling, 54:1037-1047.

Tian, X., Rao, F., Leon-Patino, C., Song, S., 2020. Effects of aluminum on the expansion and microstructure of alkali-activated MSWI fly ash-based pastes, Chemosphere, 240:124986.

Tzanakos, K., Mimilidou, A., Anastasiadou, K., Stratakis, A., Gidarakos, E., 2014. Solidification/stabilization of ash from medical waste incineration into geopolymers. Waste Manage. 34: 1823–1828.

Wang, F., Zhang, F., Chen, Y., Gao, J., Zhao, B., 2015. A comparative study on the heavy metal solidification/stabilization performance of four chemical solidifying agents in municipal solid waste incineration fly ash. Journal of Hazardous Materials, 300:451-458.

Wang, P., Hu, Y., Cheng, H., 2019. Municipal solid waste (MSW) incineration fly ash as an important source of heavy metal pollution in China. Environmental Pollution, 252:461-475.

480 Wongsa, A., Boonserm, K., Waisurasingha, C., Sata, V., Chindaprasirt, P., 2017. Use of municipal solid waste
481 incinerator (MSWI) bottom ash in high calcium fly ash geopolymer matrix. Journal of Cleaner Production,
482 148:49-59.
483 Ye, N., Chen, Y., Yang, J., Liang, S., Hu, Y., Xiao, B., Huang, Q., Shi, Y., Hu, J., Wu, X., 2016. Co-disposal of
484 MSWI fly ash and bayer red mud using an one part geopolymeric system. Journal of Hazardous Materials,
485 318: 70-78.
486 Zhan, X., Wang, L., Hu, C., Gong, J., Xu, T., Li, J., Yang, L., Bai, J., Zhong, S., 2018. Co-disposal of MSWI
487 fly ash and electrolytic manganese residue based on geopolymeric system. Waste Management 82:62–70.
488 Zhan, X., Wang, L., Wang, L., Wang, X., Gong, J., Yang, L., Bai, J., 2019. Enhanced geopolymeric co-disposal
489 efficiency of heavy metals from MSWI fly ash and electrolytic manganese residue using complex alkaline
490 and calcining pre-treatment, Waste Management, 98:135-143.
491 Zhao, S., Muhammad, F., Yu, L., Xia, M., Huang, X., Jiao, B., Lu, N., Li, D., 2019. Solidification/stabilization
492 of municipal solid waste incineration fly ash using uncalcined coal gangue-based alkali-activated
493 cementitious materials, Environmental Science and Pollution Research, 26(25): 25609-25620.
494 Zheng, L., Wang, C., Wang, W., Shi, Y., Gao, X., 2011. Immobilization of MSWI fly ash through
495 geopolymerization: effects of water-wash. Waste Management, 31(2): 311-317.
496

497 Table 1 The test mixtures for MSWI fly ash and coal fly ash geopolymers with the ratio of NaOH (8M) to
498 solid at 0.37 mL/g (Coal fly ash, CFA; MSWI fly ash, FA; Treated MSWI fly ash, TFA).

Geopolymers	CFA (wt%)	FA(wt%)	TFA(wt%)
GP-CFA	100	0	0
CFA5FA	95	5	0
CFA15FA	85	15	0
CFA20FA	80	20	0
CFA25FA	75	25	0
CFA15TFA	85	0	15
CFA20TFA	80	0	20
CFA25TFA	75	0	25

499

500

501 Table 2 Physicochemical properties of coal fly ash (CFA), MSWI fly ash (FA) and treated FA (TFA).

Chemical composition (wt%)									
Sample	SiO_2	Al_2O_3	CaO	Fe_2O_3	Na_2O	K_2O	TiO_2	SO_3	Cl
CFA	34.0	21.5	4.34	14.7	0.67	1.20	2.84	1.40	0.02
FA	5.78	2.27	22.0	1.10	9.17	12.2	0.78	21.0	8.5
TFA	16.9	2.64	29.0	2.00	1.48	0.57	2.00	29.7	0.1

Heavy metals (mg/kg)									
Sample	Cd	Cr	Cu	Mn	Ni	Pb	Zn		
CFA	<2	15.2±2.0	18.3±1.3	125±2.0	6.1±1.1	40.4±2.0	8.5±1.1		
FA	279±6.0	125±2.0	1080±19	472±8.9	35.3±1.2	6080±258	34460±1520		
TFA	9.5±0.3	96±3.0	330±4.0	163±5.4	22.1±1.0	6900±265	6710±439		

Leaching concentrations of heavy metals (mg/L)									
Sample	Cd	Cr	Cu	Mn	Ni	Pb	Zn	Cl-	Final pH
CFA	<0.02	0.04±0.002	<0.02	<0.02	<0.02	0.02±0.003	<0.02	4.0±0.15	13.0±0.02
FA	<0.02	0.57±0.02	<0.02	<0.02	<0.02	3.9±0.51	1.8±0.13	7310±125	12.0±0.01
TFA	0.35±0.003	0.05±0.01	6.7±0.06	1.2±0.08	0.13±0.006	1.1±0.02	54±0.62	41±3.4	4.7±0.1
LV[a]	0.1	1.5	5.0	2.0	1.0	1.0	2.0	-	-

502 [a] Limit value in GB8978-1996: Integrated wastewater discharge standard.
503

Table 3 The reactivity of Al and Si in raw materials for geopolymers under different temperatures (Coal fly ash, CFA; MSWI fly ash, FA; treated MSWI fly ash, TFA).

elements	Temperature (℃)	CFA	FA	TFA
Al (mg/L)	25	62.4±1.7	180.7±2	69.0±1.12
	80	694±12.3	320±1.6	138±2.1
Si (mg/L)	25	116±3.9	296±1.3	1050±11.5
	80	2500±8.6	738±8.1	1300±5.3
Si/Al moral ratio	25	1.79	1.58	14.7
	80	3.47	2.22	9.08

Table 4 The leaching test (mg/L) of coal fly ash geopolymers with raw and pretreated MSWI fly ash at 7 and 28 days (FA, MSWI fly ash; TFA, treated MSWI fly ash; the middle number is the proportion of fly ash)

Curing time	Leaching	GP-CFA	CFA5FA	CFA15FA	CFA20FA	CFA25FA	CFA15TFA	CFA20TFA	CFA25TFA
7 days	Cr	*	*	0.10±0.002	*	*	0.093±0.002	*	*
	Mn	*	*	0.04±0.002	0.035±0.002	*	0.04±0.007	0.031±0.001	*
	Cd	*	*	*	0.03±0.001	*	*	0.042±0.002	0.034±0.0025
	Zn	*	0.023±0.003	0.025±0.004	*	*	*	*	*
	Pb	*	*	*	*	*	*	*	*
	Ni	*	*	0.432±0.013	*	*	0.46±0.08	*	*
	Cu	*	*	*	*	*	*	*	*
	Cl^-	7.9±0.3	184±15	849±11	1020±18	1500±31	8.1±0.03	9.5±0.21	8.8±0.12
	pH	12.6±0.05	12.5±0.03	12.4±0.02	12.1±0.02	12.2±0.04	11.9±0.04	11.8±0.03	11.9±0.02
28 days	Cr	*	0.026±0.002	*	*	*	*	*	0.08±0.006
	Mn	0.023±0.002	0.026±0.002	0.04±0.002	0.025±0.005	0.029±0.001	0.031±0.001	0.023±0.001	*
	Cd	*	*	0.025±0.001	*	0.035±0.001	0.03±0.002	0.027±0.002	0.043±0.001
	Zn	*	0.028±0.003	0.022±0.002	0.022±0.004	*	*	*	0.024±0.002
	Pb	*	*	*	*	*	*	*	0.097±0.01
	Ni	*	*	*	*	*	*	*	*
	Cu	*	*	*	*	*	*	*	*
	Cl^-	6.2±1.7	173±10	850±16.5	1070±0.5	1330±22	6.7±0.31	8.2±0.11	8.2±0.06
	pH	12.2±0.04	12.2±0.03	12.1±0.01	12.1±0.05	12.0±0.03	11.7±0.02	11.8±0.01	12.4±0.04

* represents the value was below 0.02 mg/L.

512 Table 5 Mobility index of heavy metal in geopolymers at curing 7 and 28 days.

Curing time	Leaching	CFA5FA	CFA15FA	CFA20FA	CFA25FA	CFA15TFA	CFA20TFA	CFA25TFA
7 days	Cr	0	1.17	0	0	11.7	0	0
	Mn	*	*	*	*	0.22	0.13	0
	Cd	*	*	*	*	0	0.60	0.39
	Zn	0.26	0.09	0	0	0	0	0
	Pb	0	0	0	0	0	0	0
	Ni	*	*	*	*	23.6	0	0
	Cu	*	*	*	*	0	0	0
28 days	Cr	0.91	0	0	0	0	0	6.04
	Mn	*	*	*	*	0.17	0.10	0
	Cd	*	*	*	*	0.57	0.38	0.49
	Zn	0.32	0.08	0.06	0	0	0	0.002
	Pb	0	0	0	0	0	0	0.36
	Ni	*	*	*	*	0	0	0
	Cu	*	*	*	*	0	0	0

513 * represents that the leaching concentrations of raw materials were below the detect limit and this
514 calculation was meaningless.

515

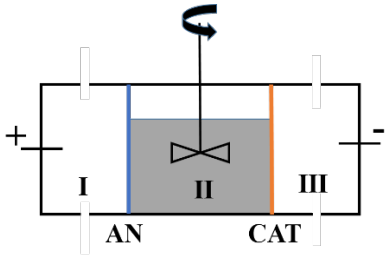

Fig. 1. The schematic figure of three-compartment electrodialytic remediation set-up (chamber I, anode chamber; AN, anion exchange membrane; chamber II, suspension chamber; CAT, cation exchange membrane; chamber III, cathode chamber).

522

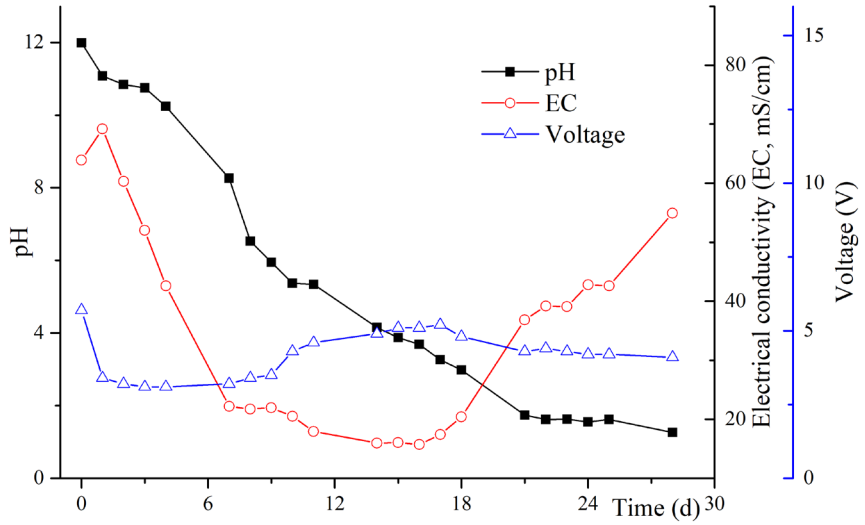

523

524 Fig. 2. The process parameters during electrodialytic pre-treatment for MSWI fly ash.

525

526

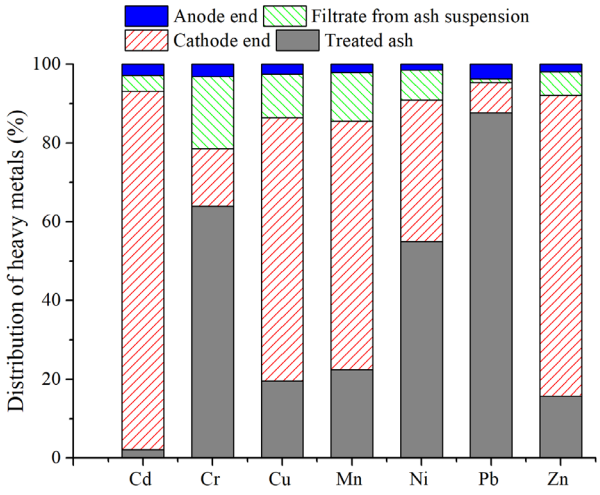

527

528 Fig. 3. The distribution of heavy metals in electrodialytic setup after electrodialytic remediation
529 experiment.

530

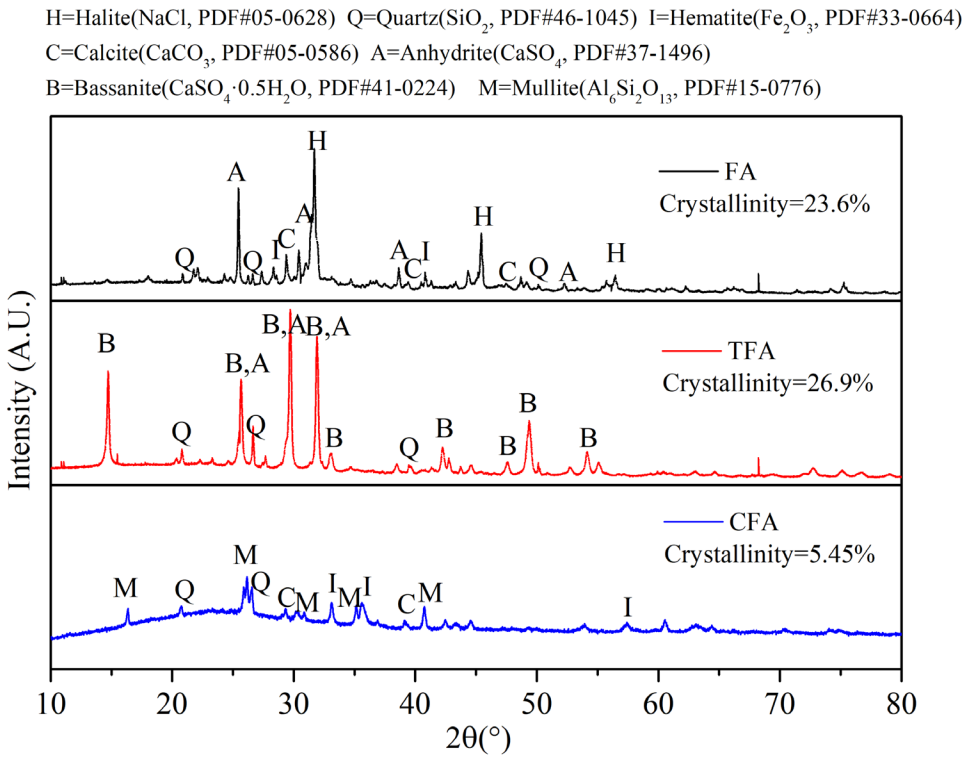

Fig. 4. XRD graphics of coal fly ash, raw and pretreated MSWI fly ash (MSWI fly ash, FA; Treated MSWI fly ash, TFA; coal fly ash, CFA).

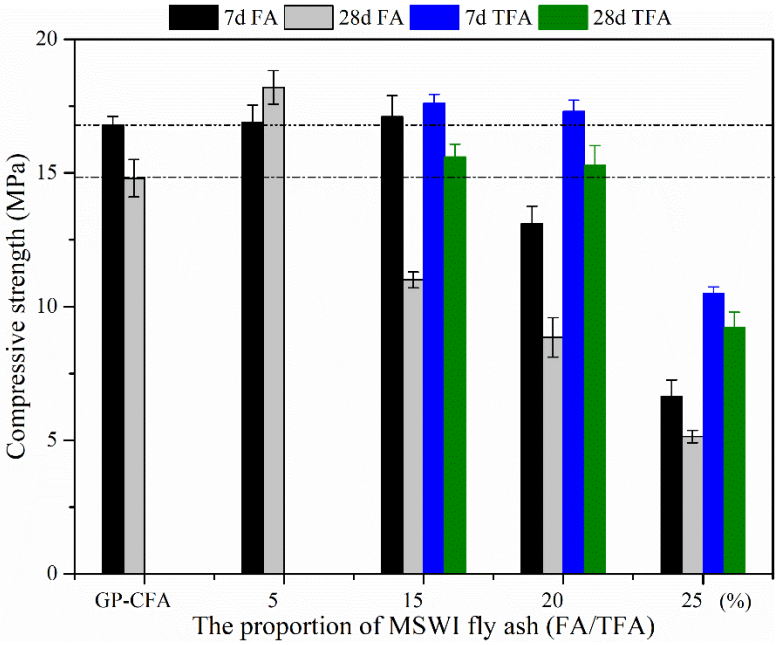

Fig. 5. The compressive strength of coal fly ash geopolymers with different initial and pretreated MSWI fly ash at 7 and 28 days.

541

M=Mullite($Al_6Si_2O_{13}$,PDF#15-0776) Q=Quartz(SiO_2,PDF#46-1045) C=Calcite($CaCO_3$,PDF#05-0586)
H=Hematite(Fe_2O_3,PDF#33-0664) F=Zeolite($Na_8(AlSiO_4)_6CO_3$,PDF#42-0214) A=Anhydrite($CaSO_4$,PDF#37-1496)
G=Gonnardite($(Ca,Na)_2(Si,Al)_5O_{10}\cdot 3H_2O$, PDF#45-1324) D=Dellaite($Ca_6(SiO_4)(Si_2O_7)(OH)_2$,PDF#29-0376)
B=Thaumasite($Ca_3Si(SO_4)_2(OH)_6\cdot 9H_2O$,PDF#44-1423) E=Calcium Silicate Hydrate($Ca_2SiO_4\cdot H_2O$,PDF#29-0373)
T=Thenardite(Na_2SO_4,PDF#37-1465) Z=Zeolite($Na_8(Al_6Si_6O_{24})S_2O_3\cdot 3H_2O$,PDF#38-0514)

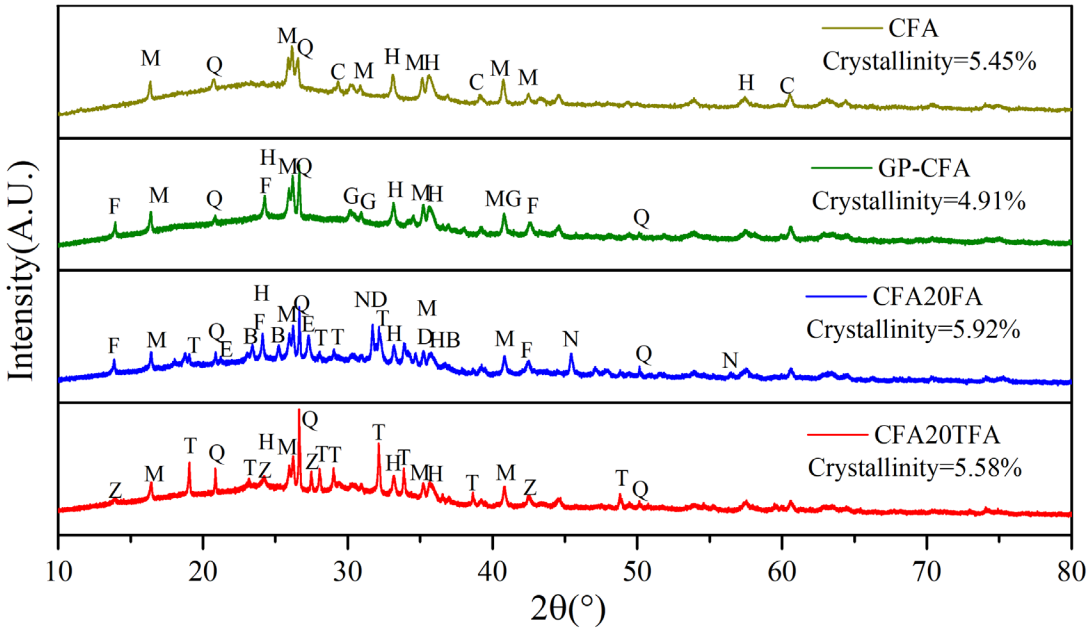

542

543 Fig. 6. XRD graphics of raw materials and geopolymers (MSWI fly ash, FA; coal fly ash, CFA; treated MSWI
544 fly ash, TFA; the middle number was the proportion of ash).

545

546

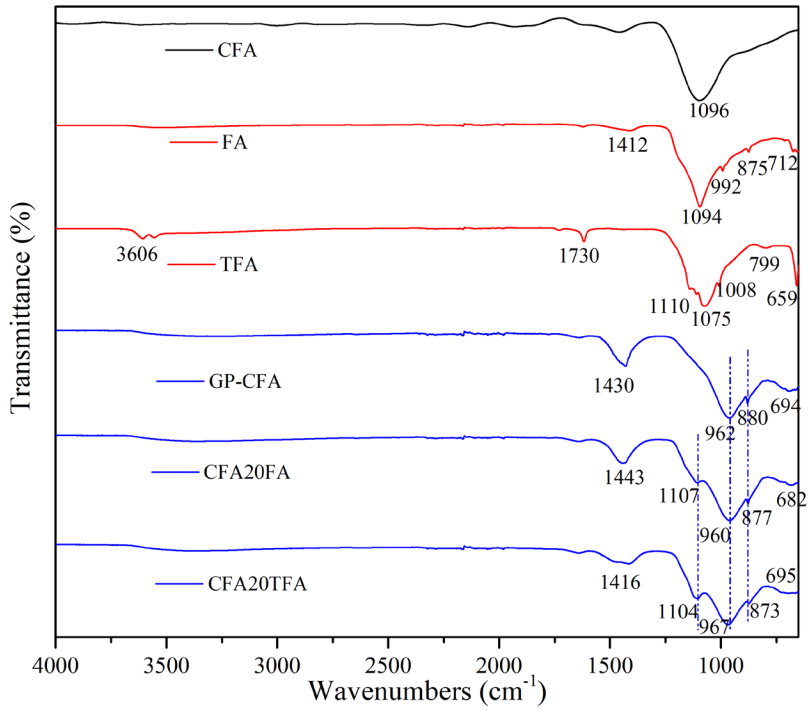

547

548 Fig. 7. FTIR graphics of raw materials and geopolymers (MSWI fly ash, FA; coal fly ash, CFA; treated MSWI
549 fly ash, TFA; the middle number was the proportion of ash).

550

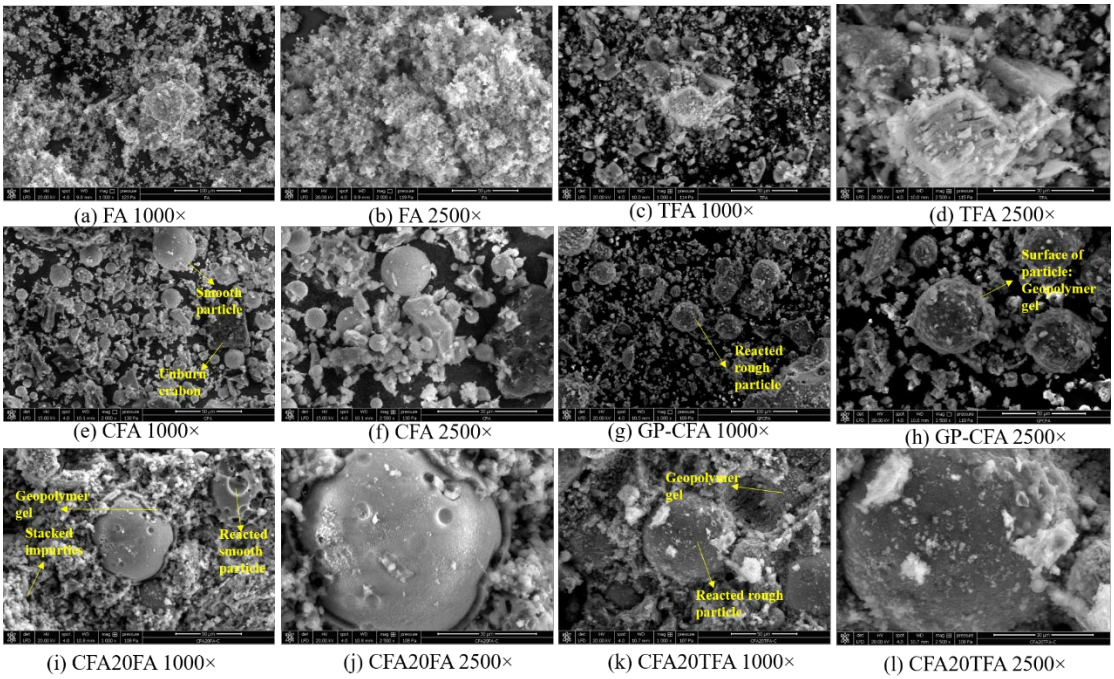

Fig. 8. SEM graphics of raw materials and geopolymers (MSWI fly ash, FA; coal fly ash, CFA; treated MSWI fly ash, TFA; the middle number was the proportion of ash).

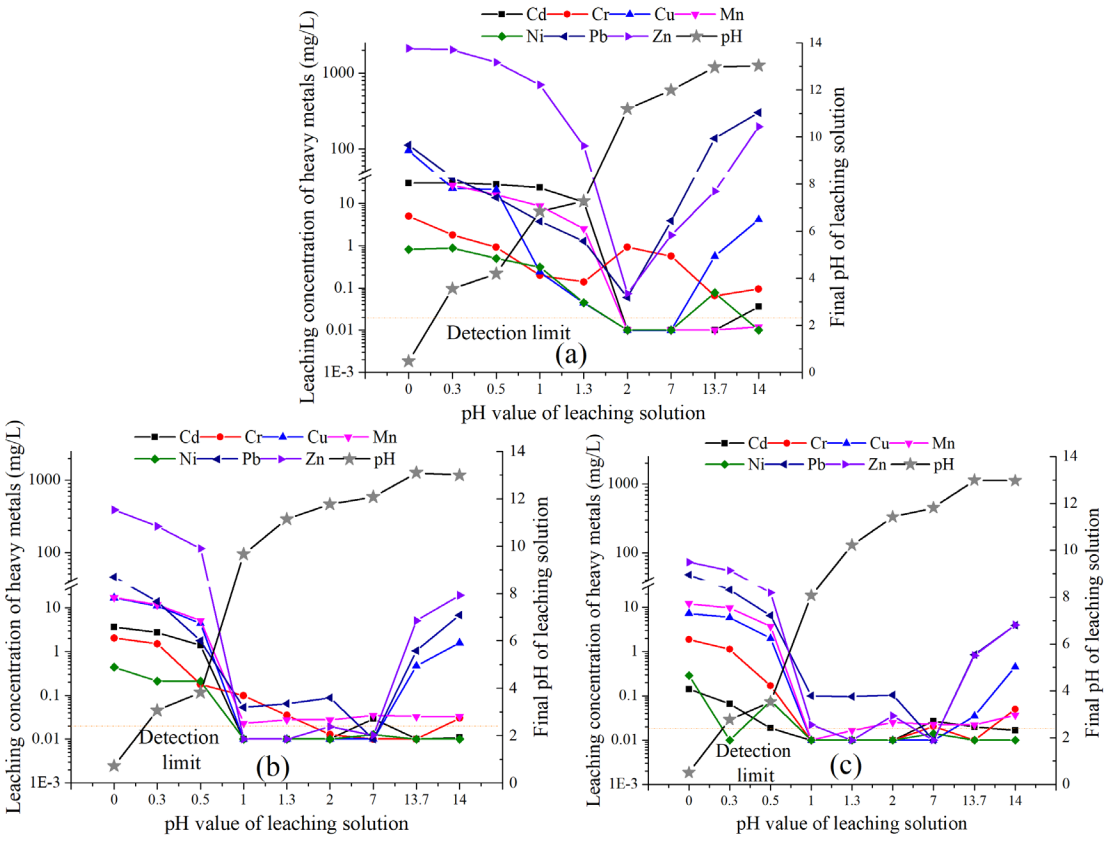

Fig. 9. The plot of pH-desorption for metals in (a) MSWI fly ash, (b) CFA20FA and (c) CFA20TFA .